

Magneto-resistivity model and valence state approximation for Ferromagnets

Andrew Das Arulsamy^{1, 2, *}

¹*Condensed Matter Group, Division of Exotic Matter, D423, Puteri Court, No.1, Jalan 28, Taman Putra, 68000 Ampang, Selangor DE, Malaysia*

²*Institute of Mathematical Sciences, University of Malaya, 50603 Kuala-Lumpur, Malaysia*

(Dated: February 16, 2019)

The magneto-transport properties, both above and below T_C of $\text{Ga}_{1-x}\text{Mn}_x\text{As}$, $\text{La}_{1-x}\text{Ca}_x\text{MnO}_3$ and $\text{Mn}_x\text{Ge}_{1-x}$ are characterized with the ionization energy based Fermi-Dirac statistics coupled with spin disorder scattering mechanism. We also highlight a simple method of predicting the minimum valence state of multi-valence Cr in $\text{La}_{0.5}\text{Pb}_{0.5}\text{Mn}_{1-x}\text{Cr}_x\text{O}_3$ using ionization energy and resistivity curves.

PACS numbers: 75.70.-i; 71.30.+h; 72.15.Rn; 75.50.Pp

Keywords: Ferromagnets, Valence state, Ionization energy, Resistivity model

I. INTRODUCTION

Diluted magnetic semiconductors (DMS) have tremendous potential for spintronics development and subsequently will lay the foundation to realize quantum computing. In order to exploit the spin assisted charge transport, one needs to understand the transport mechanism such as the variation of resistivity with temperature and doping in both paramagnetic and ferromagnetic phases. Various physical properties based on doping and Mn's valence state in manganate were reported namely, the influence of grain boundary as a barrier [1], as a region of depleted T_C [2] and polaronic effect on electrical properties [3, 4]. Direct proportionality of magnetic field, \mathbf{H} with T_C [5, 6, 7] and resistivity with defects or substrate-film lattice incompatibility [8, 9, 10, 11, 12, 13, 14, 15, 16] were also regarded as equally important to determine the electrical properties of manganate. Furthermore, metallic conduction below T_C has been studied using double exchange mechanism (DEM) between s and d orbitals [17]. The displacement of hysteresis loop in field-cooled sample with an additional scenario of non-linear spin and charge fluctuations due to magnon was reported by Solontsov *et al.* [18]. Explanations in term of hopping electrons and DEM [19], and the influence of microstructural transition arises from ionic radius or valence state of Nd in $\text{Nd}_x\text{Sm}_{1-x}\text{Ca}_{0.8}\text{MnO}_3$ [20] were also reported.

Presently, the discovery of ferromagnetism (FM) in diluted magnetic-semiconductors (DMS) such as Mn doped GaAs is expected to have an enormous impact on scientific and technological developments since both electronic and magnetic properties are realized simultaneously. Two primary advantages of DMS over manganate are the ease of controlling electrons' (n) and holes' (p) concentrations and electromigration hardly plays any significant role due to zilch oxygen content. The discovery of DMS by Munekata *et al.* [21] and later by Ohno *et al.* [22, 23] in the early 90s opened up the possibility

of having a brand new type of magneto-electronic materials other than, manganate. DMS exposes the potential applications in magnetic memory-sensors, optical isolators for optical communication systems [24] and nanotechnology [25, 26]. The progress of DMS sample growth is apparently fuelled by the advancement of Molecular-Beam-Epitaxy (MBE) technology in the 90s [27, 28, 29, 30]. Basically, FM arising from the said doped material was argued against the well known Zener DEM [31, 32] since DMS requires long-range spin interaction. This long-range spin interaction is necessary to produce FM due to very low concentration of magnetic ion (Mn) in DMS. The highest Curie temperature (T_C) has been reported to be at 110 K for MBE grown, $\text{Ga}_{0.947}\text{Mn}_{0.053}\text{As}$ compound [23]. Recently however, Teraguchi *et al.* [33] and Saito *et al.* [34] have highlighted that $\text{Ga}_{0.94}\text{Gd}_{0.06}\text{N}$ and $\text{Zn}_{0.8}\text{Cr}_{0.2}\text{Te}$ have T_C s of about 300 K and 400 K respectively. It is well known that only oxides namely, (Pr,La,Nd,Pb)-(Ca,Sr)-(Mn,Fe,Cr)-O compounds provide the established FM phenomenon with T_C ranging from above and far below room temperature (T_r). In fact, the discovery of FM in manganate were first reported by Jonker and van Santen [35, 36] in early 50s and antiferromagnetism (AFM) in $\text{Cd}_x\text{Mn}_{3-x}\text{O}_4$ by Dey [37]. This particular oxide is also captured in detail by Zener DEM [31, 32] with slight improvements in term of polaronic effect [38, 39] due to Jahn-Teller splitting of Mn^{3+} ions. However, FM with a T_C up to 110 K that was observed in Ga-Mn-As magnetic semiconductor [23] have invoked further theoretical and experimental work due to long-range spin interaction.

Several competing models have attempted to describe FM in Mn doped GaAs that includes Ruderman-Kittel-Kasuya-Yosida (RKKY) model, DEM and antiferromagnetic (AFM) superexchange mechanism as well as the Mn-holes (Mn- h) complex. The RKKY approach in the presence of the Friedel oscillations can be approximated to DEM in DMS [40]. The itinerant character of magnetic electrons and quantum oscillations (Friedel) of the electron's spin polarization around the localized spins were established for the theory of magnetic metals and the resulting competition between FM and AFM interactions

*Electronic address: sadwerdna@hotmail.com

give rise to spin-glass freezing [40, 41]. In DMS however, the mean distance between the carriers are larger than the distance between spins. Therefore, the exchange interaction mediated by the carriers in DMS favors FM rather than spin-glass freezing, which is for magnetic metals [40, 41]. Van Esch *et al.* [42, 43] have given an interpretation for FM in DMS in term of interaction between Mn ions and *holes* surrounding it in which, the Mn ions are neutral Mn^{3+} acceptors associated with $3d^5 + holes$ configuration. This neutral Mn^{3+} acceptors could be compensated by As, where for a higher concentrations of Mn, instead of replacing Ga it will form a six-fold coordinated centers with As (Mn^{6As}) [42, 43]. These centers will eventually reduce the magnitude of FM in DMS due to the loss of spin-spin interaction between $Mn(3d^5)$ and *holes*.

Interestingly, Dietl *et al.* [40, 41] have successfully incorporated both DEM and AFM superexchange mechanism into the Mn-*holes* complex in order to capture the overall mechanism involved in III-V DMS. Such incorporations are important since DEM seems to be the only mechanism that predicts T_C accurately after taking band structure effect into account [40, 41]. Note here that DMS was assumed to be charge-transfer insulators by Dietl *et al.* because *holes* from Mn^{2+} does not reside on *d* orbital but occupies an effective mass Bohr orbit with large intra-site correlation energy. Moreover, Mn ion also acts as a source of localized spin and acceptor [40]. Dietl *et al.* [40, 41] have further suggested that FM between localized spins ($S = 5/2$) of Mn is mediated by delocalized or weakly localized holes surrounding it and the resulting spin-spin interaction are indeed long range as it should be. On the other hand, the short-range AFM superexchange (if any) arises from the spin polarization of occupied electron bands (valence band). As such, AFM superexchange is mediated by short-ranged localized spins unlike FM where it requires at least weakly localized spins for long range interaction. The readers are referred to Dietl *et al.* [40] for a thorough review on DMS.

Okabayashi *et al.* [44] have pointed out convincingly that there exists an indeterminacy on pin pointing whether Mn^{2+} (negative) or Mn^{3+} (neutral) ion that dominates $Ga_{0.93}Mn_{0.07}As$ DMS. Both ions (Mn^{2+} and Mn^{3+}) were found to be favorable towards FM. In order to explain this scenario, Ando *et al.* [45] have proposed that Mn^{3+} ions populate at very low Mn concentrations due to low screening effect or large long-range Coulomb interaction. I.e., long-range Coulomb interaction will be screened-out for higher Mn concentration. Here, the changes to the Mn valence state namely, Mn^{2+} (negative) \leftrightarrow Mn^{3+} (neutral) with substitutional doping will be analyzed with ionization energy based Fermi-Dirac statistics (iFDS). Van Esch *et al.* [42, 43] have proposed multiple exchange interactions, which are ferromagnetic (FM) hole-hole and antiferromagnetic (AFM) Mn-hole interactions for DMS. These two effects, after neglecting the direct exchange between Mn-Mn (due to

very diluted nature of DMS) are seem to be sufficient enough to describe the temperature dependent magnetization curves ($M(T)$) accurately. However, even after inclusion of FM and AFM effects including the spin disorder scattering, the transition of resistivity curves with substitutional doping and temperature in both FM and paramagnetic phases are still not well understood. Unfortunately, this is also true for the case of metallic property below T_C in the well known and extensively studied FM manganate as pointed out by Mahendirian *et al.* [46]. The resistivity ($\rho(T)$) above T_C for manganate is suggested to be in an activated form described by the equation, [46]

$$\rho(T > T_C) = \rho_0 \exp\left(\frac{E_a}{k_B T}\right). \quad (1)$$

E_a is the activation energy, ρ_0 and k_B denote the residual resistivity at $T \gg E_a$ and Boltzmann constant respectively. In the FM phase, the influence of $M(T)/M_0$ is more pronounced than the electron-phonon (*e-ph*) contribution where the latter requires an overwhelmingly large coupling constant [46]. Note that M_0 is the magnitude of magnetization at 0 K. Mahendirian *et al.* have suggested that conventional mechanism namely, *e-ph* scattering cannot be used to explain $\rho(T)$ for manganate below T_C . On the contrary, $\rho(T)$ with *e-ph* involvement for DMS in the paramagnetic phase is given by [42, 43]

$$\rho(T > T_C) = \frac{C_1 + C_2 [\exp(\Theta_D/T) - 1]^{-1}}{k_B T \ln [1 + \exp((E_m - E_f)/k_B T)]}. \quad (2)$$

The term, $C_2/[\exp(\Theta_D/T) - 1]$ takes care of the *e-ph* contribution. Θ_D , E_f , E_m , C_1 and C_2 represent the Debye temperature, Fermi level, mobility edge and numerical constants respectively. On the other hand, $\rho(T)$ in the FM phase based on the spin disorder scattering as derived by Tinbergen-Dekker is given by [47]

$$\begin{aligned} \rho_{SD}(T < T_C) = & \frac{(m_{e,h}^*)^{5/2} N(2E_F)^{1/2}}{\pi(n,p)e^2\hbar^4} J_{ex}^2 \\ & \times \left[S(S+1) - S^2 \left(\frac{M_{TD}(T)}{M_0} \right)^2 - S \left(\frac{M_{TD}(T)}{M_0} \right) \right. \\ & \left. \times \tanh \left(\frac{3T_C M_{TD}(T)}{2TS(S+1)M_0} \right) \right]. \end{aligned} \quad (3)$$

N is the concentration of nearest neighbor ions (Mn's concentration) while (n, p) is the concentration of charge carriers (electrons or holes respectively). $m_{e,h}^*$ denotes the effective mass of electrons or holes, $\hbar = h/2\pi$, h = Planck constant. e is the charge of an electron, E_F and J_{ex} are the Fermi and FM exchange interaction energies respectively while S is the spin quantum number. Equation (3) equals to Kasuya [48] if one replaces the term, $\tanh[3T_C M_{TD}(T)/2TS(S+1)M_0]$ with 1. Again, a resistivity equation that can be used to

explain the transition of $\rho(T, x)$ is still lacking since spin disorder scattering alone is insufficient as shown by Tinbergen and Dekker [47] as well as reviewed by Ohno [49]. There are theories that qualitatively capture the conductivity at $T = 0$, $T < T_C$ and at $T \approx T_C$ as well as the responsible ferromagnetic interactions namely, the Kohn-Luttinger kinetic exchange (KLKE) model and the semiclassical Boltzmann (SB) model [50, 51, 52, 53, 54, 55]. In contrast, our primary intention here is to demonstrate a new method that can be used to explain the transition of the resistivity curves ($T > 0$, $T < T_C$, and $T > T_C$) with substitutional doping. This method can be extended to calculate the minimum valence state of multi-valence Cr dopant from the measured resistivity curves. However, this method cannot be used to predict T_C nor the interactions responsible for FM. This method will make use of the ionization energy based hamiltonian and Fermi-Dirac statistics. We will first derive a resistivity formula for ferromagnets for both paramagnetic and FM phases. The E_I based Fermi-Dirac statistics (iFDS) and spin disorder scattering based resistivity models will be employed in order to derive ρ as a function of T , E_I and $M_\rho(T, M_0)$. The consequences of $\rho(T, E_I, M_\rho(T, M_0))$ are discussed in detail based on the experimental data reported by Van Esch *et al.* [42, 43], Mahendiran *et al.* [46], Banerjee *et al.* [56, 57, 58, 59] and Park *et al.* [60]. The Mn_xGe_{1-x} FM semiconductor (FMS) is also accentuated here due to its promising properties for device applications [60] where its gate voltage of ± 0.5 V is compatible with the present Complementary Metal-Oxide-Semiconductor (CMOS) and Ge's hole mobility ($110.68 \text{ m}^2\text{V}^{-1}\text{s}^{-1}$) is higher than GaAs ($12.65 \text{ m}^2\text{V}^{-1}\text{s}^{-1}$) and Si ($15.81 \text{ m}^2\text{V}^{-1}\text{s}^{-1}$). Mn_xGe_{1-x} 's resistivity is also semiconductor-like below T_C , which is more suitable than metallic $Ga_{1-x}Mn_xAs$. Moreover, Mn_xGe_{1-x} is also the simplest two-element system that can be utilized to evaluate the performance of the derived model consists of iFDS and $M_\alpha(T)$ (originates from τ_{SD}). $\alpha = K$ (calculated from the Kasuya's spin disorder scattering model), ρ (calculated from the resistivity model), \exp (determined experimentally).

II. IONIZATION ENERGY BASED HAMILTONIAN

We consider the Hamiltonian with ionization energy ($H(\xi)$) as given below in order to calculate the carrier densities. The total energy in $H(\xi)$ can be directly employed to derive iFDS and subsequently, the carrier density.

$$\hat{H}\varphi = (E_0 \pm \xi)\varphi. \quad (4)$$

In Eq. (4), we define [61],

$$\pm \xi := E_{kin} - E_0 + V(x). \quad (5)$$

such that $\pm \xi$ is the energy needed for a particle to overcome the bound state and the potential that surrounds it. E_{kin} and E_0 denote the total energy at $V(x) = 0$ and the energy at $T = 0$, respectively, i.e., E_{kin} = kinetic energy. ξ is the ionization energy. The concept of ionization energy implies that [61] $\xi = E_I^{real} = E_I + V^{many body}(x)$ or $\xi = E_I + [V^{many body}(x) = 0] = E_I$. Therefore, the total energy, $E = E_0 \pm \xi = E_0 \pm E_I$ for $V^{many body}(x) = 0$ and $E = E_0 \pm \xi = E_0 \pm E_I^{real}$ for $V^{many body}(x) \neq 0$. The exact E_I values are known for an isolated atom. In this case, E_I can be evaluated with

$$E_I = \sum_i^z \frac{E_{Ii}}{z}. \quad (6)$$

However, substituting the same atom in a crystal gives rise to the influence of many-body $V(x)$ and in reality, E_I^{real} cannot be evaluated from Eq. (6). Nevertheless, the E_I^{real} of an atom or ion in a crystal is proportional to the isolated atom and/or ion's E_I as written below.

$$E_I^{real} = \alpha \sum_i^z \frac{E_{Ii}}{z} = \alpha E_I. \quad (7)$$

The $i = 1, 2, \dots, z$ represent the first, second,... ionization energies in which, z is the oxidation number of a particular ion. E_I^{real} is actually equal to the energy needed to ionize an atom or ion in a crystal such that the electron is excited to a distance r . On the other hand, the E_I is for taking that particular electron to $r \rightarrow \infty$ with $V^{many body}(x) = 0$. The constant of proportionality, α is a function of averaged $V(x)$ and varies with different background atoms. For example, in $La_{1-x}Ca_xMnO_3$ system, $La_{1-x}MnO_3$ defines the background for Ca ions. Equation (7) enables one to predict quantitatively the variation of electronic properties of magnetic semiconductors with substitution. However, the quantity E_I^{real} being unknown and using E_I instead from Eq. (6) gives the nature of approximation in $H(\xi)$. Such approximation gave remarkable predictions on the evolution of $\rho(T)$ and dielectric constant with doping in high- T_c superconductors and ferroelectrics, respectively [62, 63, 64, 65, 66, 67, 68, 69]. α in its simplest form is given by $\alpha = 1 + \frac{\langle V(x) \rangle}{E_I}$, where $\langle V(x) \rangle$ is the averaged potential. I.e., Eq. (7) suggests that even if E_I^{real} at finite r and/or $V(x)$ are not known, one can still use E_I for $r \rightarrow \infty$ in order to predict the resistivity versus temperature curves approximately. Therefore, Eq. (4) can be approximately rewritten as

$$\hat{H}\varphi \propto (E_0 \pm E_I)\varphi. \quad (8)$$

It is obvious from the hamiltonian given in Eq. (8) that we cannot use it to determine interactions responsible for FM and the magnitude of T_C , simply because we have suppressed the many body $V(x)$. However, we can employ $E_0 \pm E_I$ in order to study the kinetic properties of charge carriers since the changes in kinetic energy of charge carriers with doping, very much depend on how they are attached to the ionic core, via $\xi = \alpha E_I$. Consequently, this method was able to explain the normal state electronic transport properties of high- T_c cuprate superconductors and electronic polarization of titanate ferroelectrics [62, 63, 64, 65, 66, 67, 68, 69]. Parallel to this, from Eq. (8), the electron's and hole's distribution functions can be derived as

$$f_e(E_0) = \frac{1}{1 + \exp[\mu + \lambda(E_0 + E_I)]}, \quad (9)$$

$$f_h(E_0) = \frac{1}{1 + \exp[-\mu - \lambda(E_0 - E_I)]}. \quad (10)$$

The parameters μ and λ are the Lagrange multipliers. $\hbar = h/2\pi$, h = Planck constant and m is the charge carriers' mass. In the standard FDS, Eqs. (9) and (10) are simply given by, $f_e = 1/(1 + \exp[\mu + \lambda E])$ and $f_h = 1/(1 + \exp[-\mu - \lambda E])$.

III. RESISTIVITY MODEL BASED ON *i*FDS

The total current in semiconducting ferromagnets with contributions from both paramagnetic and FM phases is $J = \sum_{\nu} J_{\nu}$, $\nu = e^{\downarrow}, se^{\uparrow}, h^{\downarrow}, sh^{\uparrow}$. For convenience, the spin-up, \uparrow denotes the direction of the magnetic field or a particular direction below T_C , while the spin-down, \downarrow represents any other directions. Note that the total energy (Kinetic + Magnetic), $E_{K+M}^{\uparrow} \neq E_{K+M}^{\downarrow}$ due to energy level splitting below T_C . As such, the total current can be simplified as $J = J_e^{\downarrow} + J_{se}^{\uparrow} = J_e + J_{se}$ if the considered system is an *n*-type while $J = J_h + J_{sh}$ if it is a *p*-type. J_e and J_h are the spin independent charge current (electrons and holes respectively) in the paramagnetic phase whereas J_{se} and J_{sh} are the spin-assisted charge current in the FM phase. Thus the total resistivity (*n* or *p*-type) can be written as

$$\begin{aligned} \rho^{-1} &= \rho_{e,h}^{-1} + \rho_{se,sh}^{-1} \\ &= \left[\frac{m_{e,h}^*}{(n,p)e^2\tau_e} \right]^{-1} + \left[\frac{m_{e,h}^*}{(n,p)e^2\tau_{SD}} \right]^{-1}. \end{aligned} \quad (11)$$

τ_{SD} represents the spin disorder scattering rate. The carrier density for the electrons and holes (*n*, *p*) based on *i*FDS (Eqs. (9) and (10)) are given by [62, 63, 64, 65, 66, 67, 68, 69] (after taking $\exp[\mu + \lambda(E_0 + E_I)] \gg 1$)

$$n = \int_0^{\infty} f_e(E_0) N_e(E_0) dE_0$$

$$= 2 \left[\frac{k_B T}{2\pi\hbar^2} \right]^{3/2} (m_e^*)^{3/2} \exp \left[\frac{E_F - E_I}{k_B T} \right]. \quad (12)$$

$$\begin{aligned} p &= \int_{-\infty}^0 f_h(E_0) N_h(E_0) dE_0 \\ &= 2 \left[\frac{k_B T}{2\pi\hbar^2} \right]^{3/2} (m_h^*)^{3/2} \exp \left[\frac{-E_F - E_I}{k_B T} \right]. \end{aligned} \quad (13)$$

$N_{e,h}(E_0)$ is the density of states and E_F is defined from now onwards as the Fermi level at $T = 0$ so as to comply with Eq. (4). Substituting $1/\tau_e = AT^2$ (due to electron-electron interaction), Eqs. (3) and (12) or (13) into Eq. (11), then one can arrive at

$$\rho_{e,se}(T) = \frac{AB \exp[(E_I + E_F)/k_B T]}{AT^{3/2}[M_{\rho}(T, M_0)]^{-1} + BT^{-1/2}}. \quad (14)$$

In which, $A = [A_{e,h}/2e^2(m_{e,h}^*)^{1/2}][2\pi\hbar^2/k_B]^{3/2}$, $B = 2m_{e,h}^* N(\pi E_F)^{1/2} J_{ex}^2 / e^2 \hbar k_B^{3/2}$ and $\tau_{SD}^{-1} = [N(2E_F)^{1/2}(m_{e,h}^*)^{3/2}/\pi\hbar^4] J_{ex}^2 M_{\rho}(T, M_0)$. $A_{e,h}$ is the T independent electron-electron scattering rate constant. The empirical function of the normalized magnetization is given by

$$M_{\rho}(T, M_0) = 1 - \frac{M_{\rho}(T)}{M_0}. \quad (15)$$

Equation (15) is an empirical function that directly quantifies the influence of spin alignments in the FM phase on the transport properties of charge and spin carriers in accordance with Eq. (14). In other words, the only way to obtain $\frac{M_{\rho}(T)}{M_0}$ is through Eq. (15). In fact, Eq. (15) is used to calculate $M_{TD}(T)/M_0$ and $M_K(T)/M_0$ by writing $S(S+1) - S^2 \left(\frac{M_{TD}(T)}{M_0} \right)^2 - S \left(\frac{M_{TD}(T)}{M_0} \right) \tanh \left[\frac{3T_C M_{TD}(T)}{2TS(S+1)M_0} \right] = M_{\rho}(T, M_0)$ and $S(S+1) - S^2 \left(\frac{M_K(T)}{M_0} \right)^2 - S \left(\frac{M_K(T)}{M_0} \right) = M_{\rho}(T, M_0)$ respectively. Consequently, one can actually compare and analyze the $M_{\alpha}(T)/M_0$ ($\alpha = TD, K, \rho$) calculated from Tinbergen-Dekker (TD), Kasuya (K) and Eq. (14) with the experimentally measured $M_{exp}(T)/M_0$. However, one has to switch to Eq. (16) given below for the hole-doped strongly correlated paramagnetic semiconductors, which is again based on *i*FDS, [62, 63, 64, 65, 66, 67, 68, 69]

$$\rho_h = \frac{A_h(m_h^*)^{-1}}{2e^2} \left[\frac{2\pi\hbar^2}{k_B} \right]^{3/2} T^{1/2} \exp \left[\frac{E_I + E_F}{k_B T} \right]. \quad (16)$$

A_h is the T independent electron-electron scattering rate constant. Equation (16) will be used to justify the importance of the term J_{se} even if the resistivity is semiconductor-like in the FM phase. Note that, $m^* = m_e^* \approx m_h^* \approx (m_e^* m_h^*)^{1/2}$ is used for convenience. If however, $m_e^* \neq m_h^*$, then one just has to use the relation, m^*

$= m_e^* m_h^* / (m_e^* + m_h^*)$. Even in the usual consideration for the total conductivity, $\sigma = \sigma_{electron} + \sigma_{hole}$, some algebraic rearrangements can lead one to the relation, $\rho(T) \propto \exp(E_I/k_B T) / [\exp(E_F/k_B T) + \exp(-E_F/k_B T)]$, exposing the consistent effect of E_I on transport properties.

IV. DISCUSSION

A. Temperature-dependent resistivity curves

Resistivity versus temperature measurement ($\rho(T)$) is the most simplest and effective method to study the transport properties. In free-electron metals, the $\rho(T)$ curves are often exploited in order to deduce the T -dependence of the scattering rates namely, τ_{e-e} and τ_{e-ph} . Such behavior are well described by the Bloch-Grüneisen (BG) formula, [70] given by

$$\rho_{BG} = \lambda_{tr} \frac{128\pi m^* k_B T^5}{ne^2 \Theta_D^4} \int_0^{\Theta_D/2T} \frac{x^5}{\sinh^2 x} dx. \quad (17)$$

λ_{tr} = electron-phonon coupling constant, n = free electrons concentration. The approximation of $\tau_{e-e}(T)$ and $\tau_{e-ph}(T)$ using Eq. (17) is valid basically because there are no other parameters that vary with T , apart from the said scattering rates. In fact, by utilizing the BG formula, one can reliably estimate that $\tau_{e-e}(T) \propto T^{-2}$ while $\tau_{e-ph}(T) \propto T^{-3 \rightarrow -5}$ for any experimentally viable Θ_D .

On the other hand, the metallic phenomenon observed in the ferromagnetic-metallic (FMM) phase below T_C in ferromagnets (FM) cannot be characterized as Fermi gas. Therefore, it is rather incorrect to extract $\tau_{e-e}(T)$, $\tau_{e-ph}(T)$ and $\tau_{magnons}(T)$ from the $\rho(T < T_C)$ curves in FM. Experimental evidences based on the photoemission, X-ray emission/absorption and extended X-ray emission fine structure spectroscopy have exposed the polaronic effect even at $T < T_C$ or in the FMM phase. [71] Consequently, the charge density (n) in FMM phase is not T independent as one would anticipate for the free-electron metals (Fermi-gas). In addition, spin related mechanisms, like magnons and spin disorder scattering can be correctly represented with the normalized magnetization function, $M(T, M_0)$. It is quite common to employ Matthiessen's rule ($\tau^{-1} = \sum_i \tau_i^{-1}$) as opposed to the total current rule ($\tau = \sum_i \tau_i$) and write the resistivity below T_C in the form of

$$\rho(T) = \rho_0 + \sum_i A_i T^{\alpha_i}. \quad (18)$$

The i here indicates the types of T -dependent scattering rate that contribute to the resistivity and A is a T independent constant. ρ_0 is the T -independent scattering rate that originates from the impurities as $T \rightarrow$

0 K. The critical issue here is not about the validity of Matthiessen's rule, but on the validity of Eq. (18) in non free-electronic phase. Importantly, the T -dependent structure of Eq. (17) is equivalent to Eq. (18) that actually have enabled one to reliably calculate $\tau_{e-e}^{-1}(T)$ and $\tau_{e-ph}^{-1}(T)$ as $A_{e-e} T^2$ and $A_{e-ph} T^{3 \rightarrow 5}$ respectively. Equation (18) is extremely popular and it is applied indiscriminately to determine the T -dependence of a wide variety of scattering rates in FMM phase, while the correctness of such determination is still unclear and varies from one researcher to another [46, 56, 57, 58, 59]. In addition, only a free-electronic FMM phase at $T < T_C$ will justify the analysis based on Eq. (18). The influence of polaronic effect and magnetization function (the variation of $M(T)/M_0$ with T) reinforces the T -dependence of charge density, which point towards the inapplicability of Eq. (18) in FMM phase.

B. $\text{Ga}_{1-x}\text{Mn}_x\text{As}$

Oiwa *et al.* [72], Matsukura *et al.* [73], Dietl *et al.* [74] and Iye *et al.* [75] have done detailed investigations on Ga-As-Mn. The variation of electrical resistivities with temperature and doping for $\text{Ga}_{1-x}\text{Mn}_x\text{As}$ in Refs [72, 73, 74] (sample A1) differ slightly from Ref [75] (sample B2). It has been reported that the maximum T_C is ~ 70 K for $\text{Ga}_{0.957}\text{Mn}_{0.043}\text{As}$ [75] whereas $\text{Ga}_{0.947}\text{Mn}_{0.053}\text{As}$ had a $T_C \sim 100$ K. Apart from T_C , there is a switch-over in the variation of $\rho(T, x)$ where $\rho(T, x)$ decreases with x initially before switching to increasing $\rho(T, x)$ with x . $\rho(T, x)$'s variation for sample A1 is $\rho(T, 0.015) > \rho(T, 0.022) > \rho(T, 0.071) > \rho(T, 0.053) > \rho(T, 0.043) > \rho(T, 0.035)$ while for sample B2, $\rho(T, 0.015) > \rho(T, 0.022) > \rho(T, 0.071) > \rho(T, 0.035) > \rho(T, 0.043) > \rho(T, 0.053)$. The initial reduction of $\rho(T)$ with x is due to E_I ($\text{Mn}^{3+} = 1825 \text{ kJmol}^{-1} < E_I$ ($\text{Ga}^{3+} = 1840 \text{ kJmol}^{-1}$)), i.e. it supports that Mn^{3+} substitutes at Ga^{3+} sites. However, $\rho(T)$'s switch-over (from decreasing to increasing with x) at critical concentrations, $x_{c1} = 0.035$ and $x_{c2} = 0.053$ for samples A1 and B2 respectively can be explained if one employs the mechanism proposed by Van Esch *et al.* [42, 43] and Ando *et al.* [45] in which, Mn^{6A_s} formations is substantial above x_c in such a way that Mn^{3+} ions do not substitute Ga^{3+} ions. Therefore, $\rho(T)$ will be influenced by Mn^{6A_s} clusters, defects and Ga-Mn-As phase simultaneously significantly above x_c . Alternatively, using iFDS based resistivity model, one can estimate that $\text{Mn}^{2+,3+}$ do not substitute Ga^{3+} because $E_I(\text{Mn}^{2+,3+}) < E_I(\text{Ga}^{3+})$. I.e., if $\text{Mn}^{2+,3+}$ substitute Ga^{3+} then, $\rho(T)$ should decrease with x . All the values of E_I discussed above (including in the subsequent sections) were averaged in accordance with Eqs. (6) and (7). Prior to averaging, the 1st, 2nd, 3rd and 4th ionization energies for all the elements mentioned above were taken from Ref. [76].

The resistivity measurements [42, 43] and its fittings based on Eqs. (14) and (16) are shown in Fig. 1 a) and b) respectively for $\text{Ga}_{1-x}\text{Mn}_x\text{As}$. One needs two fitting

parameters (A and E_I) for $\rho(T > T_C)$ and another two (B and $M_\rho(T, M_0)$) for $\rho(T < T_C)$. All the fitting parameters are listed in Table I. Note that $S = 1$ and $5/2$ are employed for the fittings of $M_K(T)/M_0$ while T_C and $T_{crossover} = T_{cr}$ were determined from the experimental resistivity curves. The deviation of $M_K(T)/M_0$ from the M_{exp}/M_0 increases with S from $1 \rightarrow 5/2$. Equations (14) and (16) predict that if Mn^{2+} ($E_I = 1113 \text{ kJmol}^{-1}$) or Mn^{3+} ($E_I = 1825 \text{ kJmol}^{-1}$) substitutes Ga^{3+} ($E_I = 1840 \text{ kJmol}^{-1}$), then $\rho(T)$ should further decrease with x , which is not the case here. Thus, Mn^{2+} or Mn^{3+} do not substitute Ga^{3+} , in accordance with van Esch and Ando [42, 43, 45]. The T_{cr} s observed in $Ga_{0.940}Mn_{0.060}As$ (annealed: 370°C) and $Ga_{0.930}Mn_{0.070}As$ (as grown) are 10 K and 12 K , respectively, which are identical with the calculated values of 8 K and 12 K , respectively from Eq. (14). Note here that $E_I + E_F = T_{cr}$. The calculated carrier density using $E_I + E_F = 8 \text{ K}, 12 \text{ K}$, $m_h^* = \text{rest mass}$ and Eq. (13) is $2.4 \times 10^{19} \text{ cm}^{-3}$.

Figure 1 c) and d) indicate the normalized magnetization, $M_\alpha(T)/M_0$. Note that $M_{\rho,TD,K}(T)/M_0$ is a fitting parameter that has been varied accordingly to fit $\rho(T < T_C)$. Equation (15) is used to calculate $M_{\rho,TD,K}(T)/M_0$ with $S = 1$. $M_{\rho,TD,K}(T)/M_0$ is also compared with the experimentally determined [42, 43] $M_{exp}(T)/M_0$ as depicted in Fig. 1 d). One can easily notice the inequality, $M_{TD}(T)/M_0 > M_K(T)/M_0 > M_\rho(T)/M_0 > M_{exp}(T)/M_0$ from Fig. 1 c) and d). As such, $M_\rho(T)/M_0$ from Eq. (14) is the best fit for the experimentally measured $M_{exp}(T)/M_0$.

C. $\text{La}_{1-x}\text{Ca}_x\text{MnO}_3$

Mahendiran *et al.* [46] discussed $\rho(T < T_C)$ with respect to Eq. (1) and obtained the activation energy, $E_a = 0.16 \text{ eV}$ for $x = 0.1$ and 0.2 of $\text{La}_{1-x}\text{Ca}_x\text{MnO}_3$ samples at 0 T . Using Eq. (14) however, $E_I + E_F$ for $x = 0.1$ and 0.2 samples are calculated to be 0.12 and 0.11 eV respectively. The calculated carrier density, using rest mass and Eq. (13) gives 10^{17} cm^{-3} . In the presence of $\mathbf{H} = 6 \text{ T}$, $E_I + E_F = 0.0776 \text{ eV}$ for $x = 0.2$ and $p = 10^{18} \text{ cm}^{-3}$. It is proposed that the activated behavior for $\rho(T > T_C)$ is due to E_I . The fittings are shown in Fig. 2 a) and b) while its fitting parameters are listed in Table I. Theoretically, [62, 63, 64, 65, 66, 67, 68, 69] Ca^{2+} ($E_I = 868 \text{ kJmol}^{-1}$) $< \text{La}^{3+}$ ($E_I = 1152 \text{ kJmol}^{-1}$), therefore $\rho(T)$ is expected to decrease with Ca^{2+} doping significantly. On the contrary, only a small drop in $E_I + E_F$ is observed between $x = 0.1$ (0.12 eV) and 0.2 (0.11 eV) and this is due to Mn^{4+} 's compensation effect. In other words, the quantity of Mn^{4+} increased with x . In fact, the quantity of Mn^{4+} increased 6% from $x = 0.1$ (19%) to 0.2 (25%) [46]. Ideally, the difference in E_I between Ca^{2+} and La^{3+} is $1152 - 868 = 284 \text{ kJmol}^{-1}$. But, due to compensation with $6\% \text{ Mn}^{3+ \rightarrow 4+}$ ($E_I = 4940 \text{ kJmol}^{-1}$: 4^{th} ionization energy), the actual difference is only $284 - [75\%(1825) + 25\%(4940) - 81\%(1825) - 19\%(4940)] =$

97 kJmol^{-1} . 1825 kJmol^{-1} is the E_I for Mn^{3+} . This calculation simply exposes the compensation effect in which, 6% of Mn^{4+} reduces the Ca^{2+} effect from 284 kJmol^{-1} to 97 kJmol^{-1} .

At 6 T for $\text{La}_{0.8}\text{Ca}_{0.2}\text{MnO}_3$, $E_I + E_F = 78 \text{ meV}$. Figure 2 c) and d) depict the calculated $M_\alpha(T)/M_0$ with $S = 1$ and $M_{exp}(T)/M_0$ for $x = 0.2$ respectively. The calculated $M_{TD}(T)/M_0$ is dropped for $\text{La}_{1-x}\text{Ca}_x\text{MnO}_3$ since $M_K(T)/M_0$ seems to be a better approximation than $M_{TD}(T)/M_0$ as indicated in Fig. 1 c) and d). The manganate's charge transport mechanism below T_C is also in accordance with Eq. (14). Hence, Eq. (14) is suitable for both types of ferromagnets, be it diluted or concentrated.

D. $\text{La}_{0.5}\text{Pb}_{0.5}\text{Mn}_{1-x}\text{Cr}_x\text{O}_3$

Banerjee *et al.* [56, 57, 58] have proposed the existence of small polarons at $T > T_C$ in $\text{La}_{0.5}\text{Pb}_{0.5}\text{Mn}_{1-x}\text{Cr}_x\text{O}_3$ for $x = 0 \rightarrow 0.45$ using thermoelectric power and positron-annihilation lifetime measurements. They have suggested that the substitution of Cr^{3+} into Mn sites localizes e_g^1 electrons that gives rise to $\rho(T)$ [56, 57, 59]. Here, Eq. (19) as given below is used to calculate the minimum valence state of Cr from $\rho(T, x)$ curves.

$$\frac{\delta}{j} \sum_{i=z+1}^{z+j} E_{Ii} + \frac{1}{z} \sum_{i=1}^z E_{Ii} = \frac{1}{q} \sum_{i=1}^q E_{Ii}. \quad (19)$$

The first term, $\frac{\delta}{j} \sum_{i=z+1}^{z+j} E_{Ii}$ above has $i = z + 1, z + 2, \dots, z + j$ and $j = 1, 2, 3, \dots$. It is solely due to multivalence ion, for example, assume $Mn^{3+,4+}$ is substituted with Nd^{3+} ($\text{La}_{0.7}\text{Ca}_{0.3}\text{Mn}_{1-x}\text{Nd}_x\text{O}_3$) hence from Eq. (19), the first term is due to Mn^{4+} ion's contribution or caused by reaction of the form $Mn^{3+} - \text{electron} \rightarrow Mn^{4+}$ (4940 kJmol^{-1}), hence j is equals to 1 in this case and δ represents the additional contribution from Mn^{4+} . The second ($i = 1, 2, 3, \dots, z$) and last ($i = 1, 2, 3, \dots, q$) terms respectively are due to reaction of the form $Mn - 3(\text{electrons}) \rightarrow Mn^{3+}$ and $Nd - 3(\text{electrons}) \rightarrow Nd^{3+}$. Recall that $q = z = 3+$ and $i = 1, 2, 3, \dots$ represent the first, second, third, ... ionization energies while $j = 1, 2, 3, \dots$ represent the fourth, fifth, sixth, ... ionization energies. Therefore, $z + \delta$ gives the minimum valence number for Mn which can be calculated from Eq. (19). Now, it is possible to explain the doping effect in $\text{La}_{0.5}\text{Pb}_{0.5}\text{Mn}_{1-x}\text{Cr}_x\text{O}_3$ system [56, 57]. The inequalities of E_{Is} are given as Mn^{3+} (1825 kJmol^{-1}) $> \text{Cr}^{3+}$ (1743 kJmol^{-1}) and Mn^{4+} (2604 kJmol^{-1}) $> \text{Cr}^{4+}$ (2493 kJmol^{-1}). These relations strongly indicate that $\rho(T)$ should decrease with Cr^{3+} content contradicting with experimental data from Refs. [56, 57]. The only way to handle this situation is to use Eq. (19) so as to calculate the minimum valence state of $\text{Cr}^{3+\delta}$, which is $3.033+$. Actually, the valence state of Cr that substitutes Mn^{3+} is $\text{Cr}^{>3.033}$ and of course, the valence state of Mn

is fixed to be 3+. There is no need to vary it because $\rho(T)$ was found to increase with Cr content [56, 57]. Actually, higher concentration of Mn^{2+} with x will decrease $\rho(T)$ and therefore, it is unlikely. While Mn^{4+} (if any) will further increase the value of δ in $\text{Cr}^{3+\delta}$, in which both scenarios comply with iFDS via Eq. (19) and the resistivity measurements [56, 57].

E. $\text{Mn}_x\text{Ge}_{1-x}$

The $\text{Mn}_x\text{Ge}_{1-x}$ FMS with homogeneous Mn concentration has been grown using low- T MBE technique. [60] The $\text{Mn}_x\text{Ge}_{1-x}$ was found to be a *p*-type with carrier density in the order of $10^{19} - 10^{20} \text{ cm}^{-3}$ for $0.006 \leq x \leq 0.035$ as measured by Park *et al.* [60] Both the resistivity measurements [60] and its fittings based on Eq. (14) are shown in Fig. 3 a). Here, $E_I + E_F$, A and B have been floated while $M_\rho(T, M_0)$ is constrained to reduce with T in order to fit the experimental $\rho(T, x = 0.02)$. Only $1.4\text{--}1.9 \mu_B/\text{Mn}$ atom contributes to ferromagnetism as compared with the ideal value of $3.0 \mu_B/\text{Mn}$ atom, calculated by Stroppa *et al.* [77]. It is found that $E_I + E_F = 15 \text{ K}$ from the $\rho(T)$ fitting for $\text{Mn}_{0.02}\text{Ge}_{0.98}$. Therefore, the hole concentration is $2.38 \times 10^{19} \text{ cm}^{-3}$ using Eq. (13) and $m_h^* = \text{rest mass}$, which is in the vicinity of the experimental value, [60] $10^{19} - 10^{20} \text{ cm}^{-3}$. The semiconductor-like behavior of $\rho(T, x = 0.02)$ below T_C is *not* exponentially driven as indicated by Eq. (14).

The pronounced effect of Eq. (15) can be noticed by comparing the calculated plots between Eq. (14) and Eq. (14) with additional constraint, $dM_\rho(T)/dT = 0$ as indicated in Fig. 3 a). Recall that Eq. (15) is varied with T to fit the experimental $\rho(T, x = 0.02)$ in compliance with Eq. (14). Furthermore, $\rho(T)$ is found [60] to decrease with x from 0.016 to 0.02 while $\rho(T, x = 0.02)$ remains identical with $\rho(T, x = 0.033)$. This type of transition can be readily evaluated with Eq. (14). Firstly, notice the large increase in room temperature p from 10^{14} cm^{-3} (upper limit) for pure Ge to 10^{19} cm^{-3} (lower limit) for a mere 2% Mn substituted $\text{Mn}_{0.02}\text{Ge}_{0.98}$, which gives rise to a rapid decrease of $\rho(T, x)$. The average E_I s for Mn^{2+} , Mn^{3+} and Ge^{4+} are computed as 1113, 1825 and 2503 kJmol^{-1} respectively. Using iFDS, Mn substitution into Ge sites will reduce the magnitude of $\rho(T)$ since $E_I(\text{Ge}^{4+}) > E_I(\text{Mn}^{3+}) > E_I(\text{Mn}^{2+})$, regardless whether $dM(T)/dT = 0$ or $dM(T)/dT \neq 0$. Such behavior has been observed experimentally [60] where, $\rho(T, x = 0.009) > \rho(T, x = 0.016) > \rho(T, x = 0.02)$. Surprisingly however, $\rho(T, x = 0.02) \simeq \rho(T, x = 0.033)$, because one should get $\rho(T, x = 0.02) > \rho(T, x = 0.033)$. Therefore, the result, $\rho(T, x = 0.02) \simeq \rho(T, x = 0.033)$ indicates that $\text{Mn}^{2+,3+}$ ($0.033 - 0.02 = 0.013$) may not have substituted Ge, instead it could have formed a well segregated impurity phase and/or Mn^{4+} concentration have

increased with x . Notice that the formation of impurity phase or clustering in $\text{Mn}_x\text{Ge}_{1-x}$ has been predicted by Stroppa *et al.* [77], which is also common in $\text{Ga}_{1-x}\text{Mn}_x\text{As}$

FIG. 1: Equation (14) has been employed to fit the experimental $\rho(T)$ plots for $\text{Ga}_{1-x}\text{Mn}_x\text{As}$ as given in a) whereas Eq. (16) is used to fit the plots in b). All fittings are indicated with solid lines. b) is actually for annealed non-ferromagnetic $\text{Ga}_{0.930}\text{Mn}_{0.070}\text{As}$ samples. c) and d) show the T variation of calculated $M_\alpha(T)/M_{4.2}$ ($\alpha = \text{K}, \text{TD}, \rho$) with $S = 1$ for $x = 0.060$ and 0.070 respectively. $M_K(T)/M_{4.2}$ is also calculated with $S = 5/2$. The experimental $M_{\text{exp}}(T)/M_{4.2}$ plot for $x = 0.070$ (as grown) is shown in d).

FIG. 2: Experimental plots of $\rho(T)$ for $\text{La}_{1-x}\text{Ca}_x\text{MnO}_3$ at $x = 0.1, 0.2$ and 0.2 (6 T) have been fitted with Eq. (13) as depicted in a) and b). All fittings are indicated with solid lines. Whereas c) and d) show the T variation of calculated $M_\alpha(T)/M_{4.2}$ ($\alpha = \text{K}, \rho$) with $S = 1$ for $x = 0.1$ and 0.2 respectively. The experimental $M_{\text{exp}}(T)/M_{4.2}$ plot for $x = 0.2$ is given in d).

DMS with strictly limited Mn solubility. The normalized magnetization, $M_{K,\rho,\text{exp}}(T)/M_0$ for $\text{Mn}_{0.02}\text{Ge}_{0.98}$ have been plotted in Fig. 3 b).

V. CONCLUSIONS

The computed $T_{\text{crossover}}$ below T_C and carrier density in $\text{Ga}_{1-x}\text{Mn}_x\text{As}$ ($x = 6\text{--}7\%$) are 8-12 K and 10^{19} cm^{-3} , identical with the experimental values of 10-12 K and $10^{18}\text{--}10^{20} \text{ cm}^{-3}$ respectively. The calculated charge densities for $\text{Mn}_{0.02}\text{Ge}_{0.98}$ and $\text{La}_{1-x}\text{Ca}_x\text{MnO}_3$ ($x = 10\text{--}20\%$) are 10^{19} cm^{-3} and 10^{17} cm^{-3} respectively. This model can explain the evolution of resistivity's curves with respect to temperature and Mn doping. In addition, the valence state of Cr in $\text{La}_{0.5}\text{Pb}_{0.5}\text{Mn}_{1-x}\text{Cr}_x\text{O}_3$ has been estimated as $> 3.033+$. We have explained the magneto-transport properties of both concentrated and diluted ferromagnets consistently using the ionization energy based Hamiltonian and Fermi-Dirac statistics. However, this approach could not be used to calculate T_C .

Acknowledgments

The author is grateful to Kithriammah Soosay and Ronie Entili for their hospitality and financial aid. Special thanks to Bryne J.-Y. Tan, Jasper L. S. Loverio and Hendry Izaac Elim for their kind help with figure preparations and references. This project was partly funded by SAGA 66-02-03-0077 (Oracle 8150077).

FIG. 3: a) Equation (14) has been employed to fit the experimental $\rho(T)$ plots for $\text{Mn}_{0.02}\text{Ge}_{0.98}$. The plot with additional constraint, $dM_\rho(T)/dT = 0$ on Eq. (14) is also given to emphasize the influence of $M_\rho(T)/M_0$ for an accurate fitting. In these two plots, $A = 25$, $B = 1060$ and $E_I + E_F = 15$ K. The T -dependence of $\rho(T)$ in accordance with J_e only, ignoring J_{se} is calculated with Eq. (16), which lacks the ability to capture the experimental $\rho(T, x = 0.02)$. In this case, $A_h = 1.8$ and $E_I + E_F = 15$ K. Both $E_I + E_F = 15$ K and $E_I + E_F = 80$ K give p in the order of 10^{19} cm^{-3} using Eq. (13) and $m_h^* = \text{rest mass}$. b) Shows the T variation of $M_\alpha(T)/M_0$ ($\alpha = K, \rho, \exp$) for $x = 0.02$. Notice the inequality, $M_K(T)/M_0 > M_\rho(T)/M_0 > M_{\exp}(T)/M_0$ that arises as a result of the principle of least action. The T -dependence of $M_\alpha(T)/M_0$ is close to the $\text{Ga}_{1-x}\text{Mn}_x\text{As}$ DMS, rather than the traditional manganate. As such, this behavior is suspected to be associated with the multiple exchange interaction.

TABLE I: Calculated values of T independent electron-electron scattering rate constant (A), B , which is a function of T independent spin disorder scattering rate constant and spin exchange energy (J_{ex}) as well as the ionization energy (E_I). All these parameters are for Mn doped $\text{Ga}_{1-x}\text{Mn}_x\text{As}$ (as grown and annealed at 370 °C, 390 °C) and Ca doped $\text{La}_{1-x}\text{Ca}_x\text{MnO}_3$ (measured at 0 and 6 T) systems. All $\text{Ga}_{1-x}\text{Mn}_x\text{As}$ samples were measured at 0 T.

[1] S. Ju, H. Sun, Z.-Y. Li, Phys. Lett. A 300 (2002) 666.
[2] A. D. Hernandez, C. Hart, R. Escudero, O. Ares, Physica B 320 (2002) 64.
[3] E. L. Nagaev, R. M. Farzettinova, Phys. Lett. A 290 (2001) 187.
[4] D. -S. Yang, A. N. Ulyanov, M. -H. Phan, I. Kim, B. -K. Ahn, J. R. Rhee, J. S. Kim, C. Nguyen, S. -C. Yu, Physica B 327 (2003) 183.
[5] E. L. Nagaev, Phys. Lett. A 273 (2000) 258.
[6] E. L. Nagaev, Phys. Lett. A 269 (2000) 357.
[7] A. Abramovich, R. Demin, R. Koroleva, A. Michurin, K. A. Maslov, Ya. M. Mukovskii, Phys. Lett. A 259 (1999) 57.
[8] D. Rubi, S. Duhalde, M. C. Terzzoli, G. Leyva, G. Polla, P. Levy, F. Parisi, R. R. Urbano Physica B 320 (2002) 86.
[9] N. Hur, Y. Horibe, C. H. Chen, Physica B 318 (2002) 39.
[10] R. H. Heffner, J. E. Sonier, D. E. MacLaughlin, G. J. Nieuwenhuys, F. Mezei, G. Ehlers, J. F. Mitchell, S. W. Cheong, Physica B 326 (2003) 494.
[11] V. G. Prokhorov, G. G. Kaminsky, V. A. Komashko, Y. P. Lee, I. I. Kravchenko, Physica B 334 (2003) 403.
[12] W. Boujelben, A. Cheikh-Rouhou, J. Pierre, J. C. Joubert, Physica B 321 (2002) 37.
[13] W. Boujelben, A. Cheikh-Rouhou, J. Pierre, D. Abouras, J. P. Renard, K. Shimizu, Physica B 321 (2002) 68.
[14] J. R. Sun, C. F. Yeung, K. Zhao, H. K. Wong, C. M. Xiong, B. G. Shen, Physica B 334 (2003) 310.
[15] C. L. Mei, Z. P. Xiong, H. -U. Habermeier, Physica B 327 (2003) 163.
[16] A. I. Coldea, S. J. Blundell, C. A. Steer, F. L. Pratt, D. Prabhakaran, J. F. Mitchell, Physica B 326 (2003) 500.
[17] R. Demin, Koroleva, R. Szymczak, H. Szymczak, Phys. Lett. A 296 (2002) 139.
[18] A. Solontsov, C. Lacroix, Phys. Lett. A 296 (2002) 199.
[19] U. Yu, Y. Jo, B. I. Min, Physica B 328 (2003) 117.
[20] D. A. Filippov, R. Z. Levitin, A. N. Vasilev, T. N. Voloshok, R. Suryanarayanan, Physica B 327 (2003) 155.
[21] H. Munekata, H. Ohno, S. von Molnar, Armin Segmuller, L. L. Chang, L. Esaki, Phys. Rev. Lett. 63 (1989) 1849.
[22] H. Ohno, H. Munekata, T. Penney, S. von Molnar, L. L. Chang, Phys. Rev. Lett. 68 (1992) 2664.
[23] H. Ohno, A. Shen, F. Matsukura, A. Oiwa, A. Endo, S. Katsumoto, Y. Iye, Appl. Phys. Lett. 69 (1996) 363.
[24] M. Henini, III-Vs Reviews 13 (2000) 32.
[25] N. Takahashi, K. Takabayashi, E. Shirado, I. Souma, J. X. Shen, Y. Oka, J. Cryst. Growth 214-215 (2000) 183.
[26] V. F. Aguekian, N. N. Vasilev, A. Yu. Serov, N. G. Filosofov, J. Cryst. Growth 214-215 (2000) 391.
[27] H. Ohno, Adv. Colloid Interface Sc. 71-72 (1997) 61.
[28] Y. J. Park, H. T. Oh, C. J. Park, H. Y. Cho, Y. Shon, E. K. Kim, R. Moriya, H. Munekata, Current Appl. Phys. 2 (2002) 379.
[29] T. Hayashi, M. Tanaga, T. Nishinaga, H. Shimada, H. Tsuchiya, Y. Otuka, J. Cryst. Growth 175-176 (1997) 1063.
[30] T. Yasuda, M. D. Duc, Y. Segawa, J. Cryst. Growth 214-215 (2000) 159.
[31] C. Zener, Phys. Rev. 81 (1951) 440.
[32] C. Zener, Phys. Rev. 82 (1951) 403.
[33] N. Teraguchi, A. Suzuki, Y. Nanishi, Y. -K. Zhou, M. Hashimoto, H. Asahi, Solid State Commun. 122 (2002)

651.

[34] H. Saito, V. Zayets, S. Yamagata, K. Ando, *Phys. Rev. Lett.* **90** (2003) 207202.

[35] G. H. Jonker, J. H. van Santen, *Physica* **16** (1950) 337.

[36] J. H. van Santen, G. H. Jonker, *Physica* **16** (1950) 599.

[37] S. K. Dey, *Phys. Lett.* **22** (1966) 375.

[38] D. Louca, T. Egami, *Physica B* **241-243** (1998) 842.

[39] A. J. Millis, P. B. Littlewood, B. I. Shraiman, *Phys. Rev. Lett.* **74** (1995) 5144.

[40] T. Dietl, H. Ohno, F. Matsukura, *Phys. Rev. B* **63** (2001) 195205.

[41] T. Dietl, H. Ohno, F. Matsukura, J. Cibert, D. Ferrand, *Science* **287** (2000) 1019.

[42] A. Van Esch, L. Van Bockstal, J. De Boeck, G. Verbanck, A. S. van Steenbergen, P. J. Wellmann, B. Grietens, R. Bogaerts, F. Herlach, G. Borghs, *Phys. Rev. B* **56** (1997) 13103.

[43] L. Van Bockstal, A. Van Esch, R. Bogaerts, F. Herlach, A. S. van Steenbergen, J. De Boeck, G. Borghs, *Physica B* **246-247** (1998) 258.

[44] J. Okabayashi, A. Kimura, O. Rader, T. Mizokawa, A. Fujimori, T. Hayashi, M. Tanaka, *Phys. Rev. B* **58** (1998) 4211.

[45] K. Ando, T. Hayashi, M. Tanaka, A. Twardowski, *J. Appl. Phys.* **53** (1998) 6548.

[46] R. Mahendiran, S. K. Tiwary, A. K. Raychaudhuri, T. V. Ramakrishnan, R. Mahesh, N. Rangavittal, C. N. R. Rao, *Phys. Rev. B* **53**, 3348 (1996).

[47] Tineke Van Peski-Tinbergen, A. J. Dekker, *Physica* **29** 917 (1963).

[48] T. Kasuya, *Prog. Theor. Phys.* **16**, 58 (1956).

[49] H. Ohno, *Science* **281**, 951 (1998).

[50] J.M. Luttinger, W. Kohn, *Phys. Rev.* **97** 869 (1955).

[51] T. Jungwirth, M. Abolfath, J. Sinova, J. Kucera, A. H. MacDonald, *Appl. Phys. Lett.* **81** 4029 (2002).

[52] T. Jungwirth, J. Sinova, J. Macek, J. Kucera, A. H. MacDonald, *Rev. Mod. Phys.* **78** 809 (2006).

[53] E. H. Hwang, S. Das Sarma, *Phys. Rev. B* **72** 35210 (2005).

[54] M. P. Lopez Sancho, L. Brey, *Phys. Rev. B* **68** 113201 (2003).

[55] L. Brey, G. Gomez Santos, *Phys. Rev. B* **68** 115206 (2003).

[56] A. Banerjee, S. Pal, S. Bhattacharya, B. K. Chaudhuri, H. D. Yang, *Phys. Rev. B* **64** (2001) 104428.

[57] A. Banerjee, A. Sarkar, D. Sanyal, P. Chatterjee D. Banerjee, B. K. Chaudhuri, *Solid State Commun.* **125** (2003) 65.

[58] A. Banerjee, B. K. Chaudhuri, A. Sarkar, D. Sanyal, D. Banerjee, *Physica B* **299** (2001) 130.

[59] A. Banerjee, S. Pal, B. K. Chaudhuri, *J. Chem. Phys.* **115** (2001) 1550.

[60] Y. D. Park, A. T. Hanbicki, S. C. Erwin, C. S. Hellberg, J. M. Sullivan, J. E. Matson, T. F. Ambrose, A. Wilson, G. Spanos, B. T. Jonker, *Science* **295**, 651 (2002).

[61] A. Das Arul Samy, K. Ratnavelu, *physics/0702232*.

[62] A. Das Arul Samy, *cond-mat/0212202*.

[63] A. Das Arul Samy, *Physica C* **356**, 62 (2001).

[64] A. Das Arul Samy, *Phys. Lett. A* **300**, 691 (2002).

[65] A. Das Arul Samy, P. C. Ong, M. T. Ong, *Physica B* **325**, 164 (2003).

[66] A. Das Arul Samy, *Physica B* **352**, 285 (2004).

[67] A. Das Arul Samy, *Physica C* **420**, 95 (2005).

[68] A. Das Arul Samy, in: Paul S. Lewis (Ed.), *Superconductivity Research at the Leading Edge*, Nova Science Publishers, New York, 2004, pp. 45-57; A. Das Arul Samy, *cond-mat/0408613*.

[69] A. Das Arul Samy, *Phys. Lett. A* **334**, 413 (2005).

[70] J. J. Tu, G. L. Carr, V. Perebeinos, C. C. Homes, M. Strongin, P. B. Allen, W. N. Kang, E.-M. Choi, H.-J. Kim, S.-I. Lee, *Phys. Rev. Lett.* **87**, 277001 (2001).

[71] N. Mannella, A. Rosenhahn, C. H. Booth, S. Marchesini, B. S. Mun, S.-H. Yang, K. Ibrahim, Y. Tomioka, and C. S. Fadley, *Phys. Rev. Lett.* **92**, 166401 (2004).

[72] A. Oiwa, S. Katsumoto, A. Endo, M. Hirasawa, Y. Iye, H. Ohno, F. Matsukura, A. Shen, Y. Sugawara, *Solid State Commun.* **103** (1997) 209.

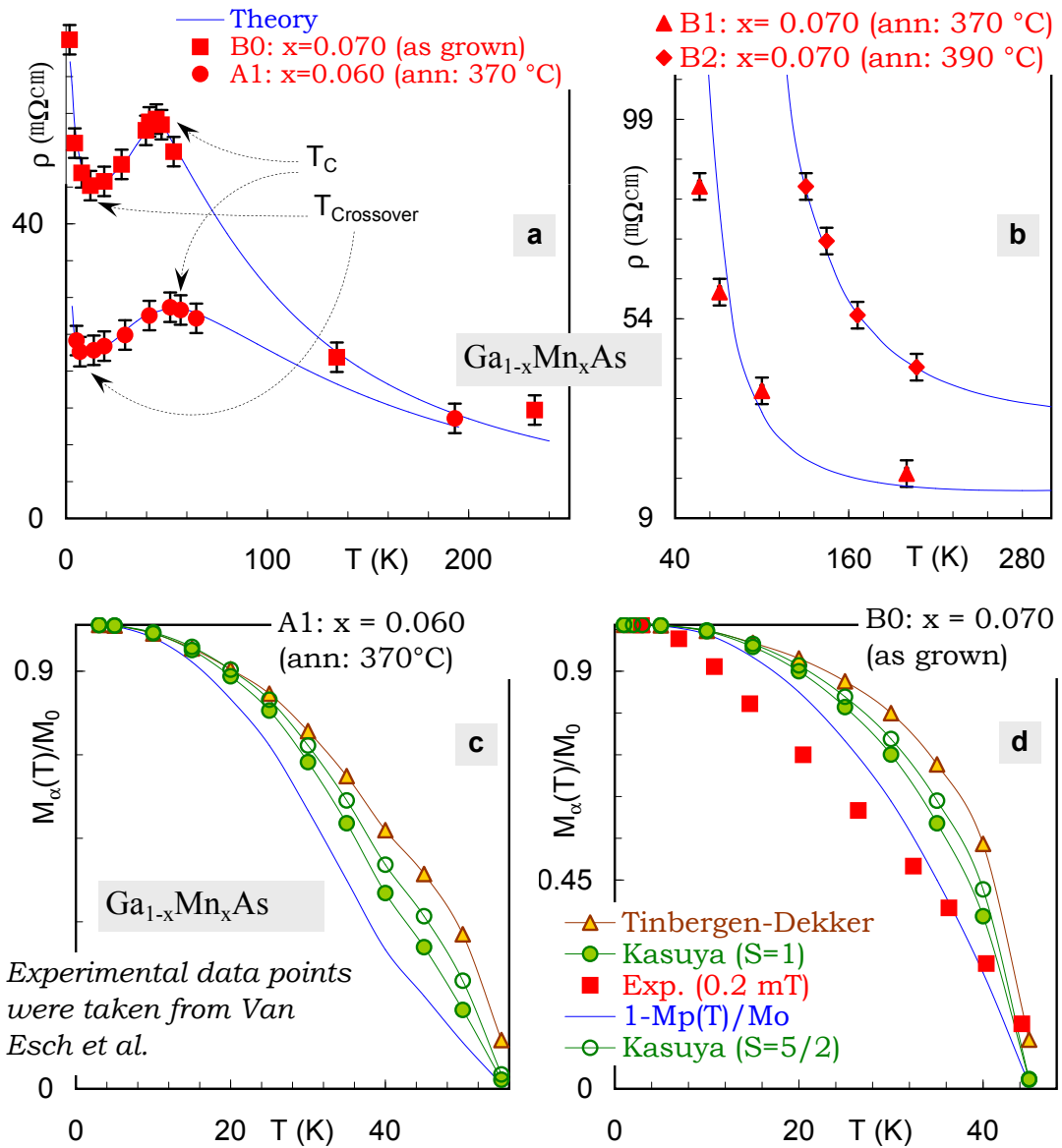
[73] F. Matsukura, H. Ohno, A. Shen, Y. Sugawara, *Phys. Rev. B* **57** (1998) 2037.

[74] T. Dietl, J. Cibert, P. Kossacki, D. Ferrand, S. Tatarenko, A. Wasiela, Y. Merle d'aubigné, F. Matsukura, N. Akiba, H. Ohno, *Physica E* **7** (2000) 967.

[75] Y. Iye, A. Oiwa, A. Endo, S. Katsumoto, F. Matsukura, A. Shen, H. Ohno, H. Munekata, *Mater. Sc. Engg. B* **63** (1999) 88.

[76] M. J. Winter (<http://www.webelements.com>).

[77] A. Stroppa, S. Picozzi, A. Continenza, A. J. Freeman, *Phys. Rev. B* **68**, 155203 (2003).



Sample ^(Ref.)	Ann. $T(H)$ °C(Tesla)	A [Calc.]	B [Calc.]	$E_I + E_F$ [Calc.] K(meV)	$T_C(T_{cr})$ K
$\text{Ga}_{0.940}\text{Mn}_{0.060}\text{As}^{(42)}$	370 (0)	4.5	400	8 (0.69)	50 (10)
$\text{Ga}_{0.930}\text{Mn}_{0.070}\text{As}^{(42)}$	As grown (0)	9.2	400	12 (1.04)	45 (12)
$\text{Ga}_{0.930}\text{Mn}_{0.070}\text{As}^{(42)}$	370 (0)	0.02	~	280 (24.2)	~
$\text{Ga}_{0.930}\text{Mn}_{0.070}\text{As}^{(42)}$	390 (0)	0.03	~	400 (34.5)	~
$\text{La}_{0.9}\text{Ca}_{0.1}\text{MnO}_3^{(46)}$	~ (0)	10	0.65	1400 (121)	222 (~)
$\text{La}_{0.8}\text{Ca}_{0.2}\text{MnO}_3^{(46)}$	~ (0)	10	1.2	1300 (112)	246 (~)
$\text{La}_{0.8}\text{Ca}_{0.2}\text{MnO}_3^{(46)}$	~ (6)	5	3.2	900 (78)	251 (~)

